scientific reports

Check for updates

OPEN

Maturity related metabolomic analysis of *Balanites aegyptiaca* fruits with in vitro and in silico cytotoxicity evaluation

Asmaa Abdelsalam[1,4]✉, Ehab Mahran[2,4], Eslam T. Mohamed[1], Arezue Boroujerdi[3] & Hebatallah Aly[1]

Balanites aegyptiaca **(L.) Delile, a medicinal tree, produces an edible fruit widely recognized in traditional medicine for its antidiabetic and liver-enhancing properties. This study investigated the metabolic changes occurring during fruit maturation using integrated nuclear magnetic resonance (NMR) metabolomics approaches, including 1D ^{1}H (proton), 2D heteronuclear single quantum coherence (HSQC), and 2D *J*-resolved NMR spectroscopy. A total of forty-five metabolites were identified and quantified, with key metabolites characterizing each maturation stage. Metabolic profiling indicated that immature fruits were characterized by elevated concentrations of amino acids, alkaloids, and organic acids, while mature fruits predominantly accumulated monosaccharides. Chemometric analyses and hierarchical clustering confirmed a significant metabolic differentiation between immature and mature fruit stages. Pathway analysis identified significant alterations predominantly in starch–sucrose metabolism, pyruvate metabolism, and the citrate cycle during maturation. Cytotoxic evaluation revealed that polar extracts from immature fruits exhibited superior cytotoxic activity against hepatocellular carcinoma cells (IC_{50} = 117.7 µg/mL) compared to mature fruit extracts (IC_{50} = 270.4 µg/mL). Molecular docking analysis further demonstrated that metabolites upregulated in immature fruits, like theophylline, showed a strong binding affinity (– 5.317 kcal/mol) to the anti-apoptotic protein BCL-2, suggesting their potential role in apoptosis regulation. This study provides insights into the metabolic dynamics during** ***Balanites aegyptiaca*** **fruit maturation, highlighting the superior therapeutic potential and significant cytotoxic activity of immature fruits compared to traditionally utilized mature fruits.**

Keywords *Balanites aegyptiaca* (L.), Fruit maturation, NMR spectroscopy, Metabolomics, Anticancer, *J*-resolved NMR

Balanites aegyptiaca (L.) Delile (*B. aegyptiaca*), commonly known as the desert date, is a drought-resistant tree species belonging to the family Zygophyllaceae. It is widely distributed across arid and semi-arid regions of Africa, the Middle East, and South Asia[1]. The plant, especially its fruit, holds a significant traditional value in folk medicine, where it has been used to treat a variety of ailments including diabetes, liver dysfunction, gastrointestinal disorders, and respiratory illnesses[2]. These therapeutic properties are largely attributed to its diverse array of bioactive compounds such as phenolic acids, flavonoids, alkaloids, and saponins which have demonstrated antioxidant, anti-inflammatory, antimicrobial, and anticancer activities[3]. Beyond its medicinal importance, the fruit is rich in essential nutrients, including vitamins, minerals, and carbohydrates[4].

Fruit maturation is a highly dynamic process that encompasses significant genetic, physiological, and biochemical changes, shaping the fruit's composition, quality, and functionality[5,6]. This maturation process is regulated by hormonal signaling molecules such as ethylene, which play a crucial role in coordinating the metabolic transitions associated with ripening. The metabolic transformations occurring during fruit maturation offer crucial insights into the biochemical pathways responsible for the development of flavor, texture, nutrients, and overall fruit quality[7]. The transition from the immature to the mature stage in fruits is marked by profound

[1]Botany and Microbiology Department, Faculty of Science, Helwan University, Cairo 11795, Egypt. [2]CAMAG Chemical Products and Adsorption Technology AG, 4132 Muttenz, Switzerland. [3]Chemistry Department, Claflin University, Orangeburg, SC 29115, USA. [4]Asmaa Abdelsalam and Ehab Mahran contributed equally to this work. ✉email: asmaa_abdulsalam@science.helwan.edu.eg

metabolic shifts, including changes in primary metabolites essential for growth and energy, as well as secondary metabolites that influence the fruit's potential bioactivities[8,9].

In arid zones such as south of Egypt, where *B. aegyptiaca* naturally grows, the growth environment is characterized by extreme conditions: prolonged drought, high solar radiation, and summer temperatures frequently exceeding 42 °C[10,11]. These conditions can lead to altered ripening patterns and stress-driven metabolic reprogramming. In this harsh habitat, accelerated fruit development and enhanced antioxidant responses are often observed as adaptive strategies to complete the reproductive cycle before critical stress thresholds are surpassed[12,13]. The distinct stress-induced metabolic pathways in medicinal desert plants remain largely unexplored, yet their investigation could provide critical insights into elucidating both the physiological and metabolomic adaptations to such extreme conditions and the pharmacological efficacy of the plant's fruit.

Metabolic profiling offers a robust approach to unravel the complex biochemical networks of medicinal plants, enabling the identification and quantification of metabolites involved in the fruit maturation process. By employing different omics approaches, it is possible to understand the molecular physiology during fruit ripening[14]. 1D NMR experiments, such as ^{1}H NMR, are predominantly utilized in metabolomic studies due to their capacity to deliver rapid and quantitative analyses of metabolite mixtures. However, the inherent complexity and peak overlap in 1D NMR spectra can obscure essential data, particularly in samples characterized by a high diversity of metabolites. 2D NMR spectra are used to enhance spectral resolution by distributing NMR signals across a secondary frequency dimension. This distribution not only clarifies overlapping peaks but can also facilitate the interpretation of coupling patterns and chemical shifts (for example, 2D *J*-resolved NMR)[15,16]. Although 1D and 2D NMR techniques provide excellent structural information and reproducibility, 2D NMR workflows typically require longer acquisition time, compared to other techniques[17].

To gain a comprehensive understanding of the metabolomic mechanisms underlying fruit ripening in extremophile plants such as *B. aegyptiaca*, it is essential to integrate NMR-based metabolomics with advanced statistical and pathway analyses. In this study, the metabolic profiling of *B. aegyptiaca* fruit ripening under the extreme environmental conditions of Aswan in Egypt, an arid region characterized by intense and prolonged drought stress, was investigated. Using high-resolution NMR-based metabolomics, stage-specific metabolites were identified to delineate the associated biochemical pathways involved in the ripening process. Furthermore, cytotoxic activity of immature and mature fruit extracts was investigated through in vitro assays and in silico docking study.

Materials and methods

Plant material

The fruits of *B. aegyptiaca* were collected in June and August 2022 from the botanical garden of Aswan University in Egypt with geographical coordinates of 24.00° N and 32.86° E. Five trees, each representing one replicate, were randomly selected. Immature fruit was collected in June 2022, whereas the mature fruit was collected in August 2022. The identification of the plant was carried out through a detailed examination of the plant's morphological characteristics, which were then compared to the literature[18]. The plant was further authenticated by Prof Hasnaa Hosni, professor of Plant Taxonomy at the Botany Department of Cairo University in Egypt and (Herbarium specimen No. HEU 011107) was kept at the herbarium of Faculty of Science, Helwan University in Egypt. The fruits collected for running the experiments were immediately immersed in liquid nitrogen and subsequently kept at − 80 °C.

Metabolite extraction

The frozen fruits were lyophilized for 24 h, and then completely homogenized. Twenty mg of each replicate was extracted using methanol, chloroform, and water in the proportions of 2:2:1.8 (*V/V/V*) based on the dry mass and water loss ratio[19,20]. Each extract was centrifuged at 5000 rpm for 5 min and the upper aqueous layer (polar extract) was separated and dried under vacuum.

NMR data collection, metabolite identification, and quantification

The dry extract was redissolved in 620 µL NMR buffer, comprising of 1 mM TMSP-d4 (deuterated trimethylsilylpropanoic acid), 100 mM sodium phosphate buffer, and 0.1% sodium azide in 99.9% D_2O. NMR data was collected using 700 MHz Bruker Avance™ III spectrometer controlled by TopSpin 3.5 software. The ^{1}H NMR spectra had a width of 16.0 ppm and 64K data points. During a 3-s recycling delay, on-resonance pre-saturation was employed to suppress the solvent. The initial increment of the pre-saturation nuclear Overhauser effect spectroscopy (pre-sat NOESY) spectra was obtained using a total of 120 scans, including 4 dummy scans, with a relaxation delay of 3 s and pre-saturation at the residual water frequency. The 90° pulse width for each sample was determined using the automatic pulse calculation experiment (pulsecal) feature in TopSpin 3.5 software (Bruker BioSpin, Billerica, MA). The data collection involved the use of a Bruker hsqcedetgpsisp 2.2 pulse sequence to acquire the ^{1}H-^{13}C HSQC data. The ^{1}H resonance was detected in the F2 dimension, exhibiting a spectral width of 16 ppm, whereas the ^{13}C resonance in the F1 dimension displayed a spectral width of 252 ppm. The acquisition of the 2D *J*-resolved NMR spectra involved 12 scans and 16 dummy scans with TD of 8192 for F2 and 40 for F1 dimension. The spectral widths used were 16 ppm in F2 dimension and 78 Hz in F1 dimension. A relaxation time of 1.0 s was utilized. The windows function was assigned to SINE for both dimensions. The sine-bell shift (SSB) was set to 0. The raw 2D *J*-resolved spectra was processed (tilted and symmetrized with respect to F1 = 0) and projected using Mnova 9.1.0 software (Mestrelab Research, S.L., USA, https://mestrelab.com/). The processed spectra were extracted using Mnova Software Suite.

Identification of metabolites was initially conducted through a comparison of the 700 MHz ^{1}H data obtained from polar extracts with the 700 MHz database available in the Chenomx NMR Suite (Edmonton, Alberta, Canada). Spectral peaks were fitted with the standards in the Chenomx database for identification. For peaks

that exhibited overlap in the proton spectra, *J* coupling constants and ^{1}H-^{13}C HSQC cross peaks were cross-referenced with previously published ^{1}H-^{13}C HSQC data and data obtained from the online sources: Human Metabolome Database (HMDB) and Biological Magnetic Resonance Bank (BMRB).

Chenomx provides the concentration of each fitted metabolite in mM based on the proportionality of the metabolite's peak area and proton equivalence to those of the internal standard, TMSP (1.0 mM). Use of a standard 1D pre-sat NOESY, which is not sensitive to small T1/T2 variation, along with controlled sample conditions (temperature and pH/buffer) ensures consistent relaxation behavior in most metabolites; thus, fitting experimental spectra to Chenomx's library of standards yields valid metabolite concentrations.

NMR data treatment and statistical and pathway analysis

Raw NMR spectra were processed using TopSpin 3.5 for alignment, baseline correction, phase correction, and chemical shift referencing to TMSP at 0.0 ppm. Spectral data were extracted from the 0.5–10.0 ppm region (excluding the water region at 4.733–4.833 ppm) with 0.01 ppm bucket widths using AMIX software 4.0 (Bruker BioSpin, Billerica, MA: https://www.bruker.com/en/products-and-solutions/mr/nmr-software/amix.html). The resulting bucket tables were exported to MetaboAnalyst 6.0[21]. Missing values were imputed as 1/5 of the minimum positive value for each metabolite to mitigate bias, followed by log transformation and autoscaling (mean-centered, unit variance) to normalize variance across features. Data preprocessing with univariate and multivariate analyses were then conducted.

The statistical analysis was based on the difference in the relative concentrations of the variables across the two fruit types. Principal component analysis (PCA) was applied to reduce dimensionality and visualize global metabolic variation. Sample clustering was assessed using Hotelling's T^2 ellipses (95% confidence intervals), and group separation significance was evaluated via permutational multivariate analysis of variance (PERMANOVA; 999 permutations). Partial least squares discriminant analysis (PLS-DA) was applied, with 95% confidence regions displayed to validate clustering robustness. Hierarchical clustering analysis (HCA) employed Euclidean distance as the similarity metric and Ward's minimum variance algorithm for dendrogram construction.

Significant metabolites (based on concentration) between the two developmental stages were identified using volcano plot analysis, combining a fold change threshold of > 2 (log2|FC|> 1) and T-tests ($p < 0.05$). To preserve the biological relevance, FC ratios were calculated using raw, non-normalized data. Features meeting both thresholds were classified as significant. The top 24 significant metabolites were visualized as boxplots, depicting relative concentrations across developmental stages.

Pathway analysis was conducted using metabolite sets from the Kyoto Encyclopedia of Genes and Genomes (KEGG) human metabolic pathways. Significantly altered metabolites were mapped to pathways via MetaboAnalyst's built-in library, and enrichment significance was assessed using a hypergeometric test. Pathway analysis was performed using *Arabidopsis thaliana* metabolic pathways as a reference. Pathway topology was weighted based on node centrality.

Cytotoxic activity against hepatocellular carcinoma

The polar extracts of both fruit types were tested for their cytotoxic activity against hepatocellular carcinoma employing the colorimetric assay Sulforhodamine B (SRB). The hepatocellular carcinoma cell line was obtained from the Nawah Scientific Laboratory, Cairo, Egypt. Cells were maintained in DMEM medium supplemented with 100 mg/mL streptomycin, 100 units/mL penicillin, and 10% heat-inactivated fetal bovine serum in a humidified, 5% (*V*/*V*) CO_2 atmosphere at 37 °C. The dried fruit extracts ($n = 3$) were solubilized in dimethyl sulfoxide (DMSO). Cell suspensions (100 µL, 5×10^3 cells) were seeded in 96-well plates and incubated for 24 h. Cells were treated with 100 µL of medium containing *B. aegyptiaca* fruit extracts at various concentrations (0.0–400 µg/mL) for 72 h. Stock solutions were prepared in DMSO and serially diluted in the culture medium to ensure the final DMSO concentration in each well was maintained at 0.1% (v/v). The medium was replaced with 150 µL of 10% trichloroacetic acid (TCA) and incubated at 4 °C for 1 h. After TCA removal and rinsing with distilled water, 70 µL of 0.4% SRB solution was added, incubated for 10 min at room temperature, and protected from light. Paclitaxel was used as a positive control. The negative control consisted of untreated cells with culture medium containing DMSO. The blank contained medium and SRB reagent without cells. Post-rinsing with 1% acetic acid and air-drying preceded the absorbance measurement at 540 nm using a FLUOstar® Omega reader after SRB dissolution in 10 mM TRIS.

Molecular docking study

Molecular docking was conducted to assess the binding interactions of metabolites from polar extracts of immature and mature *B. aegyptiaca* fruits with the anti-apoptotic protein BCL-2, using Schrödinger Maestro (version 2023-2, Schrödinger, LLC, New York, NY, USA) with the Glide module. The BCL-2 structure (PDB ID: 4LVT) was obtained from the Protein Data Bank (www.rcsb.org) and prepared using the Protein Preparation Wizard, which involved adding hydrogens, assigning bond orders, optimizing hydrogen-bond networks, removing non-essential water molecules beyond 5 Å from the active site, and minimizing with the OPLS4 force field to a root-mean-square deviation (RMSD) of 0.3 Å. From 45 statistically significant metabolites (fold change > 2, $p < 0.05$), 29 were selected for docking based on high/moderate abundance in immature fruits, reported anticancer activity or metabolic relevance to cancer, and structural feasibility (molecular weight ≤ 500 Da, suitable hydrogen bond donors/acceptors), as verified via PubChem (https://pubchem.ncbi.nlm.nih.gov). Metabolite structures were prepared using LigPrep, generating ionization states at pH 7.0 ± 2.0 with Epik, enumerating tautomers, and minimizing with OPLS4. A receptor grid (20 Å × 20 Å × 20 Å) was centered on the BCL-2 active site using Glide's Receptor Grid Generation tool. Docking was performed in Glide Extra Precision (XP) mode, retaining up to 10 poses per ligand. The protocol was validated by redocking the co-crystallized ligand (RMSD < 2 Å). Docking

scores (kcal/mol) and interactions (hydrogen bonds, salt bridges, π–cation, π–π stacking, hydrophobic contacts) were analyzed using Maestro's Pose Viewer and visualized in PyMOL (version 2.5).

Results and discussion

Metabolomic analysis of the polar extracts

The collected fruit was ellipsoid-shaped, measuring approximately 5.5 cm in length and 3.0 cm in diameter. The immature fruit exhibited a green color with a rough texture, while the mature fruit transitioned to a smooth, golden appearance, encased in a crispy exterior containing a sticky brown pulp (Fig. 1).

The average extraction yields from the immature and mature fruit were 29.0% (5.8 mg) and 30.7% (6.1 mg), respectively. A total of forty-five metabolites were identified in the polar extracts of both immature and mature fruits (Table 1). While the 1D NMR data were helpful for annotating several metabolites (Figs. S1 and S2), the verification of certain metabolites was challenging due to signal congestion and overlapping peaks, particularly in narrow spectral regions. To address these challenges, HSQC (Fig. S3) and 2D *J*-resolved (*J*-res) NMR spectroscopy were employed. The projected spectra from the *J*-res experiments enabled the precise assignment of individual compounds, which were further confirmed by the 2D *J*-res spectra (Fig. 2). The identified metabolites span various chemical classes, with sugars being the dominant group in both mature and immature fruits (Fig. S4). In the densely populated sugar region (δ_H 3.0–5.5 ppm), six sugars and sugar alcohols were assigned based on their distinct signals, including the anomeric protons.

In mature fruits, glucose and glucose-6-phosphate were the most abundant, whereas sucrose and pinitol predominated in immature fruits (Fig. S5A). This developmental shift in sugar metabolism, associated with fruit maturation, reflects a transition from sugar import and storage to enhanced glycolytic activity and metabolic readiness. While Farag et al.[22] identified sucrose as the primary sugar in *B. aegyptiaca* fruits collected from the Red Sea Governorate in Egypt, our findings highlight distinct geographical and/or metabolic variations. The accumulation of monosaccharides in mature fruits suggests enhanced glycolytic flux, possibly supporting increased energy demand and biosynthetic activity during ripening. These differences underscore the importance of considering both developmental stage and geographic origin in metabolomic profiling of *B. aegyptiaca* fruits.

Furthermore, several organic acids were identified, with malate and citrate being the most prevalent in immature fruits, while pyruvate was the most prevalent in mature fruits (Fig. S5B). Amino acids and their derivatives were detected in the fruits, with homoserine and proline being the most abundant in both maturation stages. In mature fruits, homoserine and proline were present at concentrations of 1.4 ± 0.004 mM and 2.6 ± 0.15 mM, respectively, whereas their levels were significantly increased in immature fruits, reaching 5.5 ± 0.006 mM and 5.8 ± 0.33 mM, respectively (Fig. S5C). Histamine and phenylalanine exhibited the lowest concentrations. This finding is in contrast to Cook et al.[23], who identified glutamic acid as the most abundant amino acid in *B. aegyptiaca* fruits from Niger.

Some aromatic amino acids, alkaloids and phenols such as theophylline and trigonelline, and syringate were identified in the aromatic region (Fig. S5D). Trigonelline has been previously reported in the fruits of *B. aegyptiaca*[22]. Notably, this study reports the first detection of theophylline and syringate in this species. These metabolites were not previously documented in *B. aegyptiaca*.

The polar extract obtained from the immature fruit was characterized by fifteen compounds, including asparagine, tyrosine, and valine, which were not detected in mature fruit. These amino acids are more abundant in early fruit development, playing a key role in protein synthesis[24]. It has been found that their concentration is significantly increased in immature tomato fruit compared to mature fruit[25].

γ-Aminobutyrate and threonine were detected in immature fruit but were absent in mature fruit. Conversely, glutamate was present in mature fruit but not in immature fruit. Glutamate has been recognized as a key biomarker in fruit ripening. During fruit maturity, the concentration of glutamate and its derivative, γ-aminobutyrate, undergoes substantial changes. Our findings are consistent with those of Sorrequieta et al.[26], who observed a

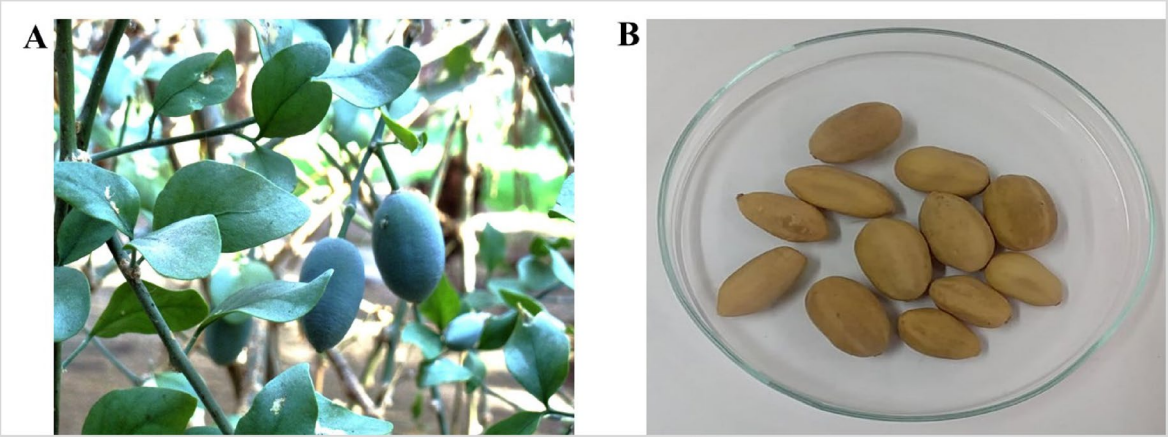

Fig. 1. Fruit of the desert date, *B. aegyptiaca* collected from Aswan, Egypt. (**A**) Immature fruit and (**B**) Mature fruit.

	Compound	Weight (g/mol)	Formula	^{13}C chemical shift (ppm) (functional group or specific C)	^{1}H chemical shift (ppm) (functional group or specific H, multiplicity of peak)	Coupling constant *J* (Hz)	Immature fruit	Mature fruit
1	1,3-Dimethylurate	196.1634	$C_7H_8N_4O_3$	30.5 (CH_3)	3.31 (CH_3, s)	–	√	√
				32.8 (CH_3)	3.44 (CH_3, s)	–		
2	5-Hydroxytryptophan	220.2246	$C_{11}H_{12}N_2O_3$	105.0 (CH)	7.11 (CH, d)	0.5	√	√
				128.2 (CH)	7.26 (CH, s)	–		
3	γ-Aminobutyrate	103.1198	$C_4H_9NO_2$	26.4 (CH_2)	1.90 (CH_2, m)	–	√	–
				37.0 (CH_2)	2.28 (CH_2, t)	7.3		
				42.0 (CH_2)	2.99 (CH_2, t)	7.4		
4	Alanine	89.0932	$C_3H_7NO_2$	53.5 (C^{α})	3.78 (H^{α}, q)	7.2, 7.2	√	√
				18.9 (C^{β})	1.46 (H^{β}, d)			
5	Acetate	60.052	$C_2H_4O_2$	26.1 (CH_3)	1.92 (CH_3, s)	–	√	–
6	Arginine	174.201	$C_6H_{14}N_4O_2$	26.6 (C^{γ})	1.64 (H^{γ}, m)	–	√	√
				30.3 (C^{β})	1.92 (H^{β}, m)	–		
				57.1 (C^{α})	3.75 (H^{α}, t)	6.2		
7	Asparagine	132.1179	$C_4H_8N_2O_3$	54.2 (C^{α})	4.01 (H^{α}, q)	4.2	√	–
				37.4 (C^{β})	2.95 (H^{β}, dd)	4.1, 17.0		
					2.88 (H^{β}, dd)	7.0, 17.0		
8	Aspartate	133.1027	$C_4H_7NO_4$	54.9 (C^{α})	3.88 (H^{α}, dd)	8.80, 2.7	√	√
				39.2 (C^{β})	2.66 (H^{β}, dd)	17.7, 8.80		
9	Betaine	117.1463	$C_5H_{11}NO_2$	69.2 (CH_2)	3.90 (H^{α}, s)	–	–	√
				56.2 (CH_3)	3.26 (H^{β}, s)	–		
10	Choline	104.1708	$C_5H_{14}NO$	58.6 (C^{α})	4.06 (H^{α}, m)	–	√	√
				56.8 (C^{γ})	3.21 (H^{γ}, s)	–		
				70.4 (C^{β})	3.52 (H^{β}, m)	–		
11	Citrate	192.1235	$C_6H_8O_7$	48.4 (CH_2)	2.52 (CH_2, d)	2.5	√	√
				48.4 (CH_2)	2.65 (CH_2, d)	2.6		
12	Dimethylamine	45.0837	C_2H_7N	37.0 (CH_3)	2.73 (CH_3, s)	–	√	√
13	Erythritol	122.1198	$C_4H_{10}O_4$	74.7 (CH)	3.66 (CH, m)	–	√	√
				65.3 (CH)	3.78 (CH, dd)	–		
14	Formate	46.0254	CH_2O_2	–	8.44 (CH, s)	–	√	√
15	Fructose	180.1559	$C_6H_{12}O_6$	78.2 (^{3}CH)	4.12 (^{3}CH, dd)	–	√	√
				66.1 ($^{6}CH_2$)	4.02 ($^{6}CH_2$, dd)	12.7, 1.0		
				72.0 (^{5}CH)	4.00 (^{5}CH, m)	7.7, 5.4		
				66.6 (^{1}CH)	3.56 (^{1}CH, m)	–		
16	Glucose	180.1559	$C_6H_{12}O_6$	98.9 ($^{1\alpha}$CH)	4.66 ($^{1\alpha}$CH, d)	7.8	√	√
				94.8 ($^{1\beta}$CH)	5.24 ($^{1\beta}$CH, d)	3.9		
				74.4 ($^{2\alpha}$CH)	3.53 ($^{2\alpha}$CH, m)	–		
				72.6 (^{4}CH)	3.41 (^{4}CH, m)	–		
				63.7 (^{6}CH)	3.74 ($^{5\beta}$CH, m)	–		
17	Glucose-6-P	260.1358	$C_6H_{13}O_9P$	94.9 (CH)	5.20 (CH, d)	3.75	√	√
				98.9 (CH)	4.60 (CH, d)	8.0		
				65.4 (CH)	4.00 (CH, m)	–		
18	Glutamate	147.1293	$C_5H_9NO_4$	29.7 (C^{β})	2.04 (H^{β}, m)	–	–	√
				36.2 (C^{γ})	2.35 (H^{γ}, m)	–		
				57.3 (C^{α})	3.74 (H^{α}, dd)	7.1, 4.7		
19	Glutamine	146.1445	$C_5H_{10}N_2O_3$	33.7 (C^{γ})	2.46 (H^{γ}, m)	–	√	√
				29.1 (C^{β})	2.14 (H^{β}, m)	–		
				57.0 (C^{α})	3.78 (H^{α}, t)	6.3		
20	Glycine	75.0666	$C_2H_5NO_2$	44.3 (C^{α})	3.56 (H^{α}, s)	–	√	–
21	Histamine	111.1451	$C_5H_9N_3$	26.7 (CH_2)	3.00 (CH_2, t)	7.12	√	–
				41.8 (CH_2)	3.29 (CH_2, t)	7.12		
				119.0 (CH)	7.09 (CH, s)	–		
				138.7 (CH)	7. 91 (CH, s)	-		
22	Homoserine	119.1192	$C_4H_9NO_3$	35.1 (C^{β})	2.10 (H^{β}, m)	–	√	√

Continued

	Compound	Weight (g/mol)	Formula	^{13}C chemical shift (ppm) (functional group or specific C)	^{1}H chemical shift (ppm) (functional group or specific H, multiplicity of peak)	Coupling constant *J* (Hz)	Immature fruit	Mature fruit
23	Isoleucine	131.1729	$C_6H_{13}NO_2$	26.8 (C^{γ})	1.29 (H^{γ}, m)	–	√	–
				17.5 (C^{γ})	1.00 (H^{γ}, d)	7.1		
				13.9 (C^{δ})	0.91 (H^{δ}, t)	7.5		
24	Lactate	90.0779	$C_3H_6O_3$	22.2 (CH_3)	1.33 (CH_3, d)	6.8	√	–
25	Leucine	131.1729	$C_6H_{13}NO_2$	24.7 (C^{δ})	0.97 (H^{δ}, d)	6.44	√	–
26	Lysine	146.1876	$C_6H_{14}N_2O_2$	32.5 (C^{β})	1.80 (H^{β}, m)	–	√	–
				41.6 (C^{ε})	3.00 (H^{ε}, t)	–		
				57.1 (C^{α})	3.70 (H^{α}, t)	6.9		
27	Malate	134.0874	$C_4H_6O_5$	45.2 (CH_2)	2.36 (CH_2, dd)	15.5, 10.3	√	√
				45.4 (CH_2)	2.65 (CH_2, dd)	15.5, 2.9		
28	Malonate	104.0615	$C_3H_4O_4$	50.2 (C^{β})	3.12 (H^{β}, s)	–	√	√
29	Methylamine	31.0571	CH_5N	27.6 (CH_3)	2.58 (CH_3, s)	–	√	–
30	Oxypurinol	152.1109	$C_5H_4N_4O_2$	128.8 (CH)	8.2 (CH, s)	–	–	√
31	Pinitol	194.183	$C_7H_{14}O_6$	62.3 (CH_3)	3.60 (CH_3, s)	9.8	√	√
				72.5 (^{1}CH)	3.82 (^{1}CH, m)	–		
				74.0 (^{2}CH)	3.56 (^{2}CH, dd)	–		
				85.8 (^{3}CH)	3.35 (^{3}CH, t)	9.8		
				74.8 (^{4}CH)	3.35 (^{4}CH, t)	4.0, 10.3		
				73.2 (^{5}CH)	3.76 (^{5}CH, dd)	4.0, 10.3		
				72.5 (^{6}CH)	3.82 (^{6}CH, m)	–		
32	Phenylalanine	165.1891	$C_9H_{11}NO_2$	39.2 (C^{β})	3.09 (H^{β}, dd)	7.0	√	–
				58.9 (C^{α})	3.99 (H^{α}, dd)	6.3		
				132.1 (C^{δ})	7.31 (H^{δ}, m)	–		
				130.4 (C^{ζ})	7.36 (H^{ζ}, m)	–		
				31.8 (C^{ε})	7.41 (H^{ε}, m)	–		
33	Proline	115.1305	$C_5H_9NO_2$	64.2 (C^{α})	4.13 (H^{α}, m)	–	√	√
				49.0 (C^{δ})	3.41 (H^{δ}, m)	–		
				31.9 (C^{β})	2.36 (H^{β}, m)	–		
34	Pyroglutamate	129.114	$C_5H_7NO_3$	27.9 (C^{γ})	2.40 (H^{γ}, m)	–	√	√
				60.9 (C^{α})	4.16 (H^{α}, dd)	–		
35	Pyruvate	88.0621	$C_3H_4O_3$	29.3 (CH_3)	2.35 (CH_3, s)	–	√	√
36	Sarcosine	89.0932	$C_3H_7NO_2$	35.5 (CH_3)	2.73 (CH_3, s)	–	√	–
				53.4 (CH_2)	3.61 (CH_2, s)	–		
37	Sucrose	342.2965	$C_{12}H_{22}O_{11}$	95.1 (^{1}CH)	5.42 (^{1}CH, d)	3.89	√	√
				79.8 ($^{3'}$CH)	4.22 ($^{3'}$CH, d)	8.8		
				76.8 ($^{4'}$CH)	4.06 ($^{4'}$CH, t)	38.6		
				73.9 (^{2}CH)	3.56 (^{2}CH, m)	–		
				72.1 (^{3}CH)	3.48 (^{3}CH, m)	–		
				65.3 ($^{6}CH_2$)	3.83 ($^{6}CH_2$, m)	–		
				64.2 ($^{1'}CH_2$)	3.69 ($^{1'}CH_2$, s)	–		
				72.1 (^{3}CH)	3.48 (^{3}CH, m)	–		
38	Succinate	118.088	$C_4H_6O_4$	37.1 (CH_2)	2.41 (CH_2, s)	–	√	–
39	Syringate	198.1727	$C_9H_{10}O_5$	109.0 (CH)	7.28 (CH, d)	1.9	√	–
				58.7 (CH)	3.90 (CH_3, s)	–		
40	Theophylline	180.164	$C_7H_8N_4O_2$	144.4 (CH)	7.98 (CH, s)	–	√	√
				32.9 (CH_3)	3.53 (CH_3, s)	–		
				30.8 (CH_3)	3.35 (CH_3, s)	–		
41	Threonine	119.1192	$C_4H_9NO_3$	63.4 (C^{α})	3.55 (H^{α}, d)	5.20	√	–
				23.0 (C^{γ})	1.33 (H^{γ}, d)	6.49		
42	Trigonelline	137.136	$C_7H_7NO_2$	148.2 (^{2}CH)	9.10 (^{2}CH, s)	8.80	√	√
				147.4 (^{4,6}CH)	8.84 (^{4,6}CH, t)	7.37		
				130.5 (^{5}CH)	8.08 (^{5}CH, t)			
				51.1 ($^{1}CH_3$)	4.42 ($^{1}CH_3$, s)			
43	Tyrosine	181.1885	$C_9H_{11}NO_3$	38.2 (C^{β})	3.10 (H^{β}, dd)	7.30, 14.30	√	–
Continued								

	Compound	Weight (g/mol)	Formula	^{13}C chemical shift (ppm) (functional group or specific C)	^{1}H chemical shift (ppm) (functional group or specific H, multiplicity of peak)	Coupling constant *J* (Hz)	Immature fruit	Mature fruit
44	Valine	117.1463	$C_5H_{11}NO_2$	63.0 (C^{α})	3.60 (H^{α}, d)	4.54	√	–
				20.8 (C^{γ})	0.98 (H^{γ}, d)	7.10		
				19.5 (C^{γ})	1.03 (H^{γ}, d)	7.10		
45	Myo-Inositol	180.1559	$C_6H_{12}O_6$	77.0 (CH)	3.30 (CH, t)	–	√	√
				73.8 (CH)	3.60 (CH, dd)	4.3, 1.8		

Table 1. Metabolites identified in the polar extract of *Balanites aegyptiaca* fruit.

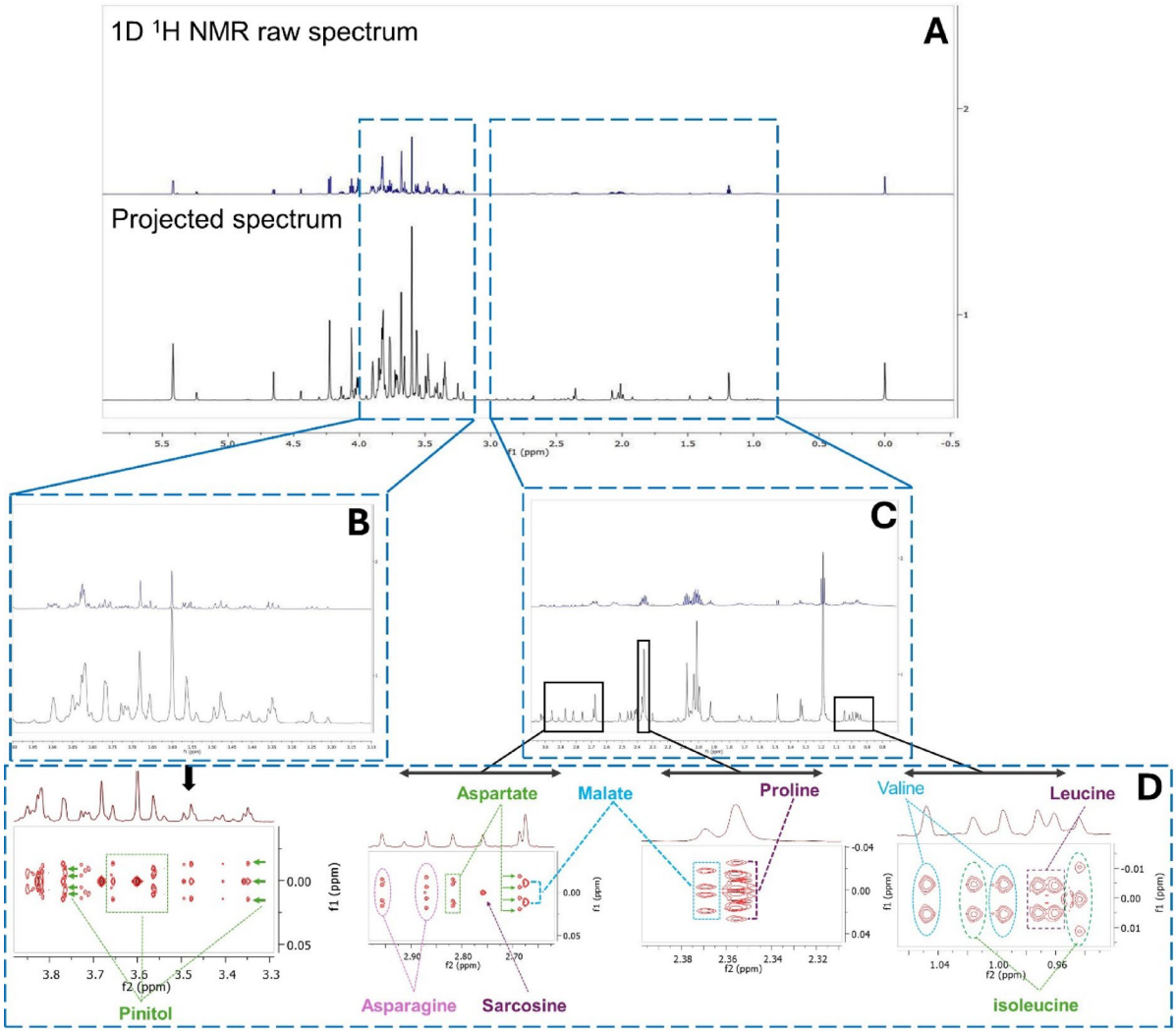

Fig. 2. *J*-resolved NMR of *Balanites aegyptiaca* polar extract. Original and projected spectra in the region δ_H 0.0–6.0 ppm (**A**); expanded regions between δ_H 0.8–3.0 ppm (**B**); and δ_H 3.1–4.0 ppm (**C**) with their respective 2D *J*-resolved NMR spectra (**D**) of identified metabolites in each region.

decrease in γ-aminobutyrate levels in ripe tomato fruit and an increase in glutamate concentration. Glutamate is the most abundant amino acid in mature tomato fruit, playing a critical role in flavor development. Its high concentration contributes to the umami taste, which is a major component of the sensory profile of ripe tomatoes[26]. The ripening process has been shown to significantly elevate glutamate levels[27]. This increase in glutamate concentration is attributed to a reduction in the activity of glutamate decarboxylase, which normally converts glutamate into γ-aminobutyrate and carbon dioxide, and an enhanced activity of GABA transaminase in mature fruit[26].

Multivariate analyses reveal distinct metabolic profiles between polar extracts of mature and immature fruits. In the unsupervised PCA model (Fig. 3A), the first two principal components collectively captured 70.4% of the total variance. Similarly, the supervised PLS-DA model (Fig. 3B), used to maximize class discrimination, showed that Component 1 and Component 2 accounted for 45.2% and 24.6% of the variance, respectively, confirming the distinct grouping between the two maturity stages. Also, Hierarchical clustering (Fig. 3C) further confirmed this differentiation. The PLS-DA biplot highlighted several metabolites that contributed significantly to the discrimination between groups along component 1. Among these, sucrose, phenylalanine, fructose, glucose, erythritol, betaine, and pyroglutamate were identified as key variables driving the separation, indicating their potential role in differentiating the metabolic profiles.

Furthermore, the volcano plot (Fig. 3D) was generated to identify potential biomarkers by integrating fold-change analysis and statistical significance (p value), with several metabolites meeting the thresholds ($|\log2FC| > 1$, $p < 0.05$). This approach enables the identification of metabolites that are not only statistically significant but also biologically relevant to the maturation process. A total of 24 metabolites were upregulated and 20 were downregulated during fruit maturation. The box plots (Fig. 4) generated based on the volcano plot analysis show the relative concentrations of the most significant metabolites.

The box plots show a higher concentration of sucrose coupled with a lower concentration of monosaccharides in immature fruit compared to mature fruit indicating the accumulation of simple sugars and a change in metabolism during ripening. This plays a role in enhancing the sweetness and flavor of the fruit[28]. The increase in monosaccharides and decrease in disaccharides in mature fruit is attributed to increased activity of hydrolytic enzymes, such as invertase and amylase. These enzymes exhibit higher activity in ripe compared to unripe fruit[29,30]. Erythritol is a sugar alcohol known for its pleasant sweetness, utilized as a sweetener in calorie-reduced foods[31]. This metabolite is characterized by several biological activities, including antidiabetic and antioxidant properties, and it can reduce plaque and potentially prevent decay of teeth[32,33].

Phenylalanine, a precursor in the phenylpropanoid pathway, plays a critical role in synthesizing secondary metabolites and defense-related compounds in pear fruit[34]. It has been also identified as a key contributor to the volatile aroma in plants[35,36]. Betaine has a role in maintaining the osmotic balance and protecting the cellular structure during stress conditions[37]. Earlier studies have demonstrated that betaine affects the antioxidant and

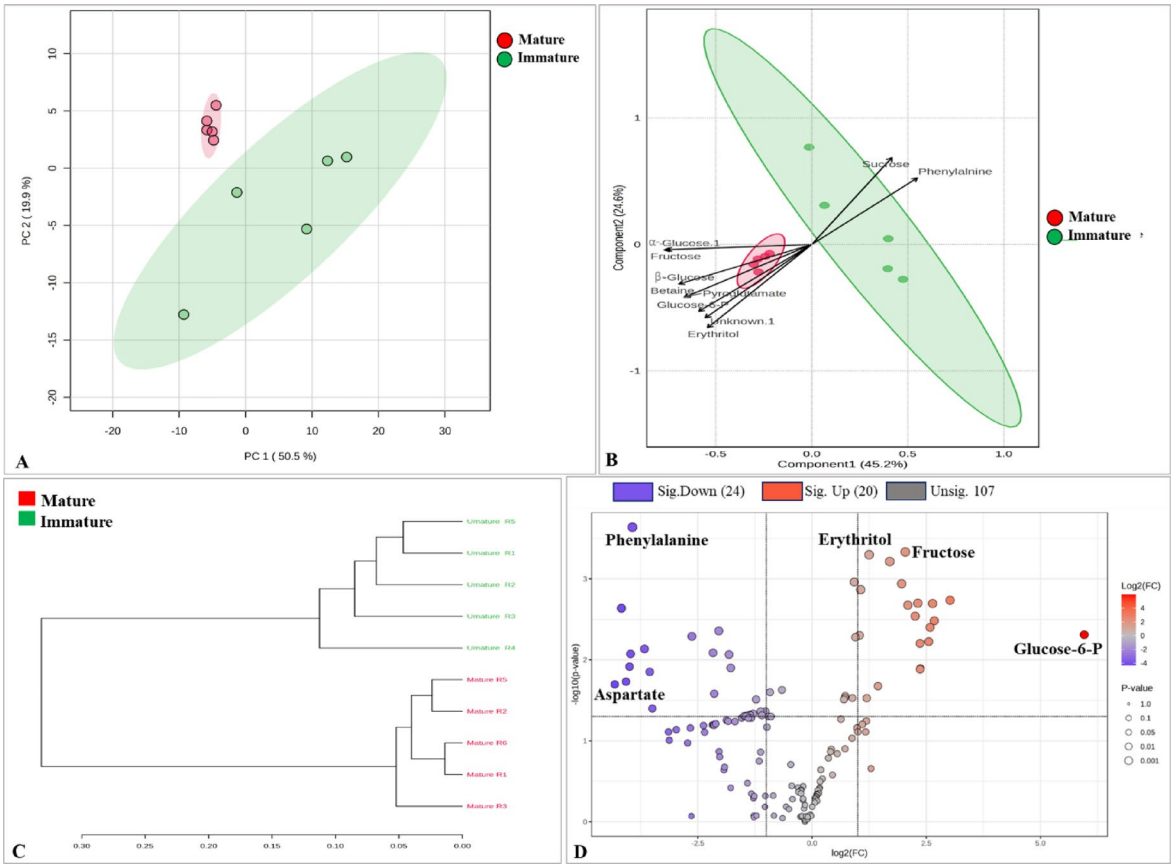

Fig. 3. Statistical analysis of metabolomic differences between immature and mature *B. aegyptiaca* fruits. (**A**) 2D score plot of PCA showing clear separation between immature and mature fruit samples; ellipses represent 95% Hotelling's confidence intervals, (**B**) PLS-DA biplot, (**C**) HCA dendrogram and (**D**) volcano plot identifying significantly different metabolites (Mature/Immature); the five most significant metabolites are labelled.

membrane fatty acid metabolism of fruits and vegetables to mitigate abiotic stress damage[38]. It has been reported to improve the flavor quality of peach fruit[39].

Based on box plot analysis, the relative quantities of amino acids arginine, proline, phenylalanine, and homoserine, were higher in immature fruit compared to mature fruit. Amino acids serve as building blocks of proteins and precursors for various secondary metabolites which are necessary for fruit maturation and protection under stress conditions. Arginine plays a crucial role in both plant development and stress tolerance. As a nitrogen-rich amino acid, arginine serves as a key nitrogen storage molecule and a precursor for polyamines, which are essential for plant growth and fruit ripening[40]. It also contributes to abiotic stress responses as a precursor of polyamines and nitric oxide, which help to stabilize membranes, and to enhance the antioxidant defense mechanisms under drought, salinity, and oxidative stresses[40,41]. Proline is known for its role in osmoprotection in mitigating abiotic stresses such as drought and high temperatures common in arid regions[42]. Phenylalanine serves as a pivotal precursor in the biosynthesis of various aroma compounds in fruits through the phenylpropanoid pathway. This pathway leads to the formation of volatile phenylpropanoids which contribute to the characteristic floral and fruity aromas of many fruits[35].

Herein, the concentrations of organic acids citrate and malate, were found to be higher in immature fruit. Citrate and malate have been identified as the predominant organic acids in a variety of fruits[43,44]. Citric acid and malic acid are known to accumulate in larger concentrations in immature fruit and serve as respiratory substrates throughout fruit ripening. Consequently, their concentrations decrease during the last stages of fruit maturation[45]. Passion fruit exhibited the highest levels of citric acid during its immature stage, which decreased as the fruit matured[46]. During grape ripening, malate released from the vacuole plays a pivotal role as the primary carbon source for energy metabolism and biosynthesis, replacing sugars.

The increased concentrations of theophylline and trigonelline in immature fruit in the present study are consistent with the findings of Pereira et al.[30], who observed a reduction in alkaloid levels with fruit development. According to Koshiro et al.[47], trigonelline exhibited more biosynthetic activity in young fruit. As the fruit matures, trigonelline is transported from the outer layer to the seeds. This process explains the drop in trigonelline concentration observed in mature fruit. Alkaloids are known to play a significant role in plant defense mechanisms by deterring herbivores and inhibiting microbial growth, which is particularly important during the vulnerable early stages of fruit development[48].

Metabolic pathway changes during fruit maturation

Significant alterations in metabolic pathways during the ripening of *B. aegyptiaca* fruit are illustrated in Fig. 5. During the transition from the immature to the mature stage, a total of thirty-nine metabolic pathways exhibited significant changes based on the pathway analysis (Table 2). Starch and sucrose metabolism, pyruvate metabolism, and the citrate cycle (TCA) pathways had particularly strong impacts between mature and immature fruit. The relationship between the significant metabolic pathways and the significant metabolites is shown in Fig. 6. The starch–sucrose metabolism pathway is of great importance among the many metabolic pathways involved in fruit ripening. This pathway controls the process of converting starch into sucrose and then to the monosaccharides glucose and fructose, which are crucial for the taste, sweet flavor, and overall fruit quality[49,50]. Moreover, the starch–sucrose metabolism pathway is intricately linked to sugar signaling mechanisms that regulate gene expression and enzymatic activities during fruit ripening[51,52]. Sugar signals can induce the expression of ethylene biosynthesis genes, thereby enhancing the ripening process[52].

The pyruvate metabolism pathway plays a central role in fruit maturity. As an end-product of glycolysis, pyruvate fuels the TCA cycle for ATP generation and organic acid metabolism, influencing fruit flavor. It also serves as a precursor for amino acids. Pyruvate serves as a precursor of acetaldehyde by the enzyme pyruvate decarboxylase, a natural aromatic component found in nearly all fruits, which accumulates throughout ripening. Acetaldehyde is a precursor to other naturally aromatic compounds[49]. Moyano et al.[50] investigated the roles of two pyruvate decarboxylase genes (Fapdc1 and Fapdc3) in strawberry fruits. The former was reported as crucial for fruit ripening and aroma biosynthesis, while the latter is implicated in overall metabolism to facilitate energy production and the biosynthesis of more complex metabolites.

The TCA cycle is a key metabolic pathway responsible for the production of organic acids and secondary metabolites that contribute to the color, taste, and flavor of mature fruit compared to immature fruit. The use of TCA flow in energy production or metabolite biosynthesis is determined by the cell's energy needs and physiological state[53–55]. According to a study by Tao et al.[56] and Li et al.[57], the TCA cycle was the predominant pathway involved in the maturation process of apple and blueberry fruit.

Cytotoxic activity of the fruit extracts against hepatocellular carcinoma

The results showed that the polar extracts of immature fruit exhibited better cytotoxic activity against hepatocellular carcinoma compared to the mature fruit, with IC_{50} values of 117.7 µg/mL and 270.4 µg/mL, respectively (Figs. 7 and S7). The IC_{50} value for the positive control, paclitaxel, was 0.15 µg/mL. Fig. S6 illustrates the morphological characteristics of cells observed under inverted microscopy. Untreated control cells exhibit a dense, compact, and well-organized structure, indicative of typical carcinoma morphology. In contrast, cells treated with paclitaxel show pronounced cytotoxic effects, including cell shrinkage, structural distortion, and markedly reduced cell density. Exposure to the polar extract of immature fruits results in significant morphological alterations, characterized by considerable structural disruption and a decrease in cell density. In comparison, cells treated with the polar extract of mature fruits lower levels of cytotoxicity, indicating a reduced antiproliferative effect relative to the immature fruit extract.

The extracts from both developmental phases are rich in bioactive metabolites with well-documented roles in cancer treatment, such as theophylline[58], trigonelline[59,60], phenylalanine[61], histamine[62], arginine[63], and D-pinitol[64,65]. We propose that the pronounced cytotoxic effects of the polar extract obtained from immature fruit,

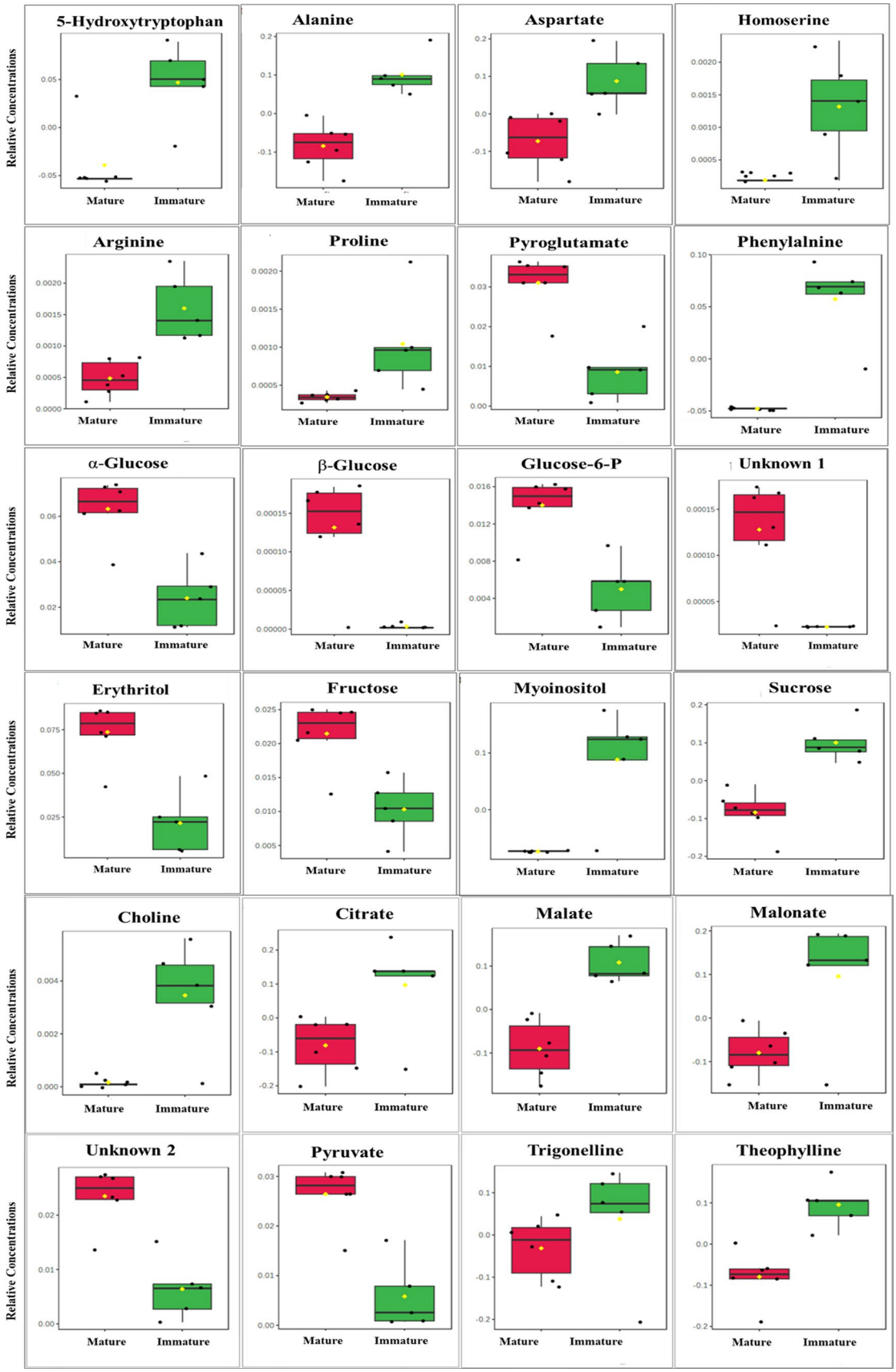

compared to the extract derived from mature fruit, are due to the higher concentrations of these metabolites in immature fruit. Moreover, the extract of immature fruit showed the presence of fifteen metabolites, many of which are well known to possess biological activities. For example, syringate has anti-inflammatory, antioxidant, and antimicrobial activities[66].

◀**Fig. 4**. Boxplots of relative concentrations of the metabolites in polar extracts from mature and immature fruit (the 24 most significant metabolites selected from Volcano plot analysis). The black dots represent the concentration of the selected metabolite in each replicate. The mean concentration of each treatment is indicated by the yellow diamond. The Y axis defines the relative abundances of the specific metabolite, and the X axis defines the treatment group.

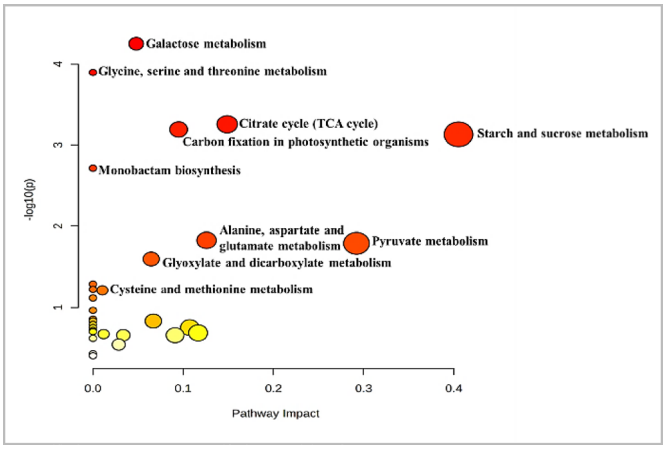

Fig. 5. Metabolic pathways in *B. aegyptiaca* that are significantly altered between mature and immature fruit based on KEGG database (www.kegg.jp/kegg/kegg1.html). The dark red circles indicate the pathways that were significantly affected. As the *p* value increases, the color progressively fades, whereas the larger the circle size, the greater the pathway's influence.

In silico study

The molecular docking study demonstrated that 29 metabolites from *B. aegyptiaca* fruit extracts interacted with the BCL-2 protein (PDB ID: 4LVT), supporting their potential cytotoxic activity. The binding poses of some compounds are visualized in Fig. 8. Theophylline exhibited the highest docking score (−5.317 kcal/mol), forming hydrogen bonds with ASN 140 and ARG 143 (Table S1), consistent with its pro-apoptotic effects[67]. Phenylalanine, detected in immature extracts, scored −4.657 kcal/mol with a hydrogen bond to ALA 97, potentially contributing to cytotoxicity via dipeptide derivatives. Trigonelline (−4.652 kcal/mol) formed a hydrogen bond with ASN 140, a salt bridge with ARG 143, and a π–cation interaction with TYR 105, aligning with its anticancer properties[59,60]. Histamine (−4.649 kcal/mol), also in immature extracts, formed a hydrogen bond with GLU 149, suggesting receptor-mediated anticancer effects[68]. Other compounds, such as asparagine (−2.992 kcal/mol), may influence cancer cell survival[69]. These findings highlight the superior bioactivity of immature fruit extracts compared to mature extracts.

The integration of metabolomics, in vitro cytotoxicity assays, and in silico molecular docking provides a powerful, multi-layered approach to understanding the therapeutic potential of *B. aegyptiaca* fruits. This study moves beyond merely cataloging the chemical constituents to functionally connecting them with biological activity. First, the identification of distinct metabolic profiles of immature and mature fruits established a chemical basis for their differential effects. The subsequent cytotoxicity assays confirmed that the higher concentration of certain alkaloids, organic acids, and amino acids in immature fruits correlates with enhanced anticancer efficacy. The in silico docking analysis provides crucial mechanistic insight, suggesting that these specific metabolites can directly interact with and inhibit key anti-apoptotic proteins like BCL-2. This synergistic approach, linking chemical composition to cellular effect and then to molecular target interaction, validates the superior therapeutic potential of immature fruits and provides a robust framework for future drug discovery efforts based on these natural products.

Conclusion

This study presents the first in-depth metabolomic investigation of *B. aegyptiaca* fruit maturation using advanced 1D and 2D NMR data, leading to the identification of 45 metabolites and significant metabolic transitions. Multivariate statistical analysis revealed clear metabolic differences between immature and mature stages. Key metabolites that characterized each stage were successfully identified. Immature fruits were characterized by elevated levels of sucrose, pinitol, malate, and citrate, whereas mature fruits showed an increase in monosaccharides and pyruvate, reflecting a metabolic shift favoring sugar hydrolysis and organic acid utilization. Pathway analyses highlighted key alterations in starch–sucrose and pyruvate metabolism, offering insights into biochemical adaptations in desert-adapted species. Notably, immature fruit extracts demonstrated higher cytotoxic activity against hepatocellular carcinoma than mature fruit. Molecular docking confirmed the interactions of some of the identified metabolites with the anti-apoptotic BCL-2 protein, supporting their apoptotic potential.

Pathway	Total	Expected	Hits	Raw p	Holm adjust	FDR	Impact
Carbon fixation	21	0.19626	4	2.62E−05	0.002433	0.002433	0.09578
Galactose metabolism	27	0.25234	4	7.43E−05	0.006833	0.003453	0.04805
Glycine, serine and threonine metabolism	33	0.30841	4	0.000168	0.015254	0.005196	0
Citrate cycle (TCA cycle)	20	0.18692	3	0.000675	0.060789	0.013987	0.15879
Alanine, aspartate and glutamate metabolism	22	0.20561	3	0.000902	0.08031	0.013987	0.1259
Starch and sucrose metabolism	22	0.20561	3	0.000902	0.08031	0.013987	0.40507
Monobactam biosynthesis	8	0.074766	2	0.002201	0.19145	0.029236	0
Pyruvate metabolism	23	0.21495	2	0.01835	1	0.21332	0.29205
Glyoxylate and dicarboxylate metabolism	29	0.27103	2	0.02852	1	0.2947	0.15112
C5-Branched dibasic acid metabolism	6	0.056075	1	0.05487	1	0.51029	0
D-Amino acid metabolism	7	0.065421	1	0.063739	1	0.5147	0
Cysteine and methionine metabolism	46	0.42991	2	0.066413	1	0.5147	0.01038
Lysine biosynthesis	9	0.084112	1	0.081245	1	0.58121	0
Selenocompound metabolism	13	0.1215	1	0.11535	1	0.67728	0
Nicotinate and nicotinamide metabolism	13	0.1215	1	0.11535	1	0.67728	0
Butanoate metabolism	17	0.15888	1	0.14827	1	0.67728	0
Arginine biosynthesis	18	0.16822	1	0.15632	1	0.67728	0
Tyrosine metabolism	18	0.16822	1	0.15632	1	0.67728	0
beta-Alanine metabolism	18	0.16822	1	0.15632	1	0.67728	0
Fructose and mannose metabolism	18	0.16822	1	0.15632	1	0.67728	0.06695
Ascorbate and aldarate metabolism	20	0.18692	1	0.17222	1	0.67728	0
Cyanoamino acid metabolism	21	0.19626	1	0.18006	1	0.67728	0
One carbon pool by folate	21	0.19626	1	0.18006	1	0.67728	0
Thiamine metabolism	22	0.20561	1	0.18783	1	0.67728	0
Valine, leucine and isoleucine biosynthesis	22	0.20561	1	0.18783	1	0.67728	0.10727
Lipoic acid metabolism	24	0.2243	1	0.20317	1	0.67728	0
Tryptophan metabolism	25	0.23364	1	0.21074	1	0.67728	0
Pantothenate and CoA biosynthesis	25	0.23364	1	0.21074	1	0.67728	0
Glycolysis or Gluconeogenesis	26	0.24299	1	0.21824	1	0.67728	0.11665
Glutathione metabolism	27	0.25234	1	0.22567	1	0.67728	0.01195
Arginine and proline metabolism	28	0.26168	1	0.23304	1	0.67728	0.03364
Inositol phosphate metabolism	28	0.26168	1	0.23304	1	0.67728	0.08958
Terpenoid backbone biosynthesis	31	0.28972	1	0.25476	1	0.71796	0
Glycerophospholipid metabolism	38	0.35514	1	0.30324	1	0.82945	0.02862
Amino sugar and nucleotide sugar metabolism	52	0.48598	1	0.39153	1	1	0

Table 2. Pathway analysis depicting significantly altered metabolic pathways in *Balanites aegyptiaca* fruit extracts. The table shows the detailed results from the pathway analysis generated with MetaboAnalyst 6.0. Since many pathways are being tested at the same time, the statistical *p* values from enrichment analysis are further adjusted for multiple testings. In particular, *Total* is the total number of compounds in the pathway; *Hits* is the matched number from the user uploaded data; *Raw p* is the original p value calculated from the enrichment analysis; *Holm p* is the p value adjusted by Holm-Bonferroni method; *FDR p* is the p value adjusted using False Discovery Rate; *Impact* is the pathway impact value calculated from pathway topology analysis.

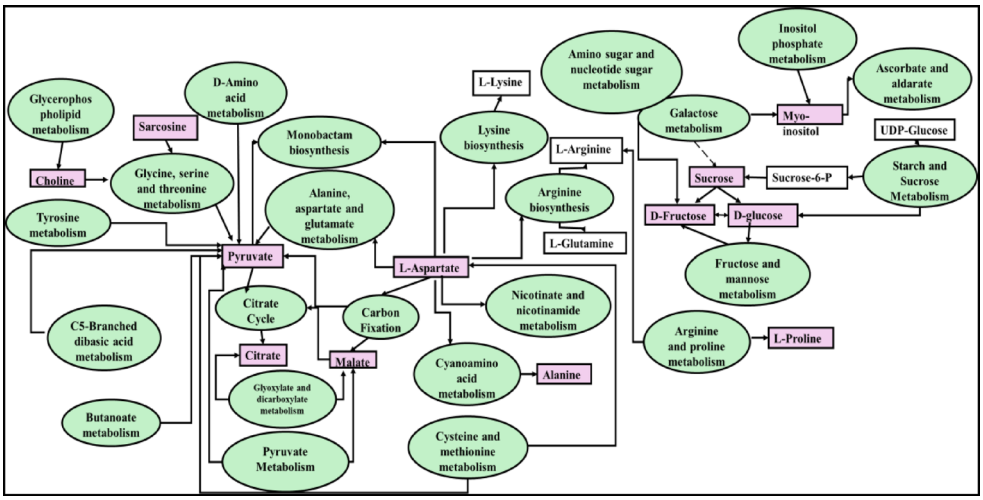

Fig. 6. Metabolic pathways that significantly changed (in green ovals) as well as the significant metabolites (in pink squars) that changed between immature and mature *B. aegyptiaca* fruits.

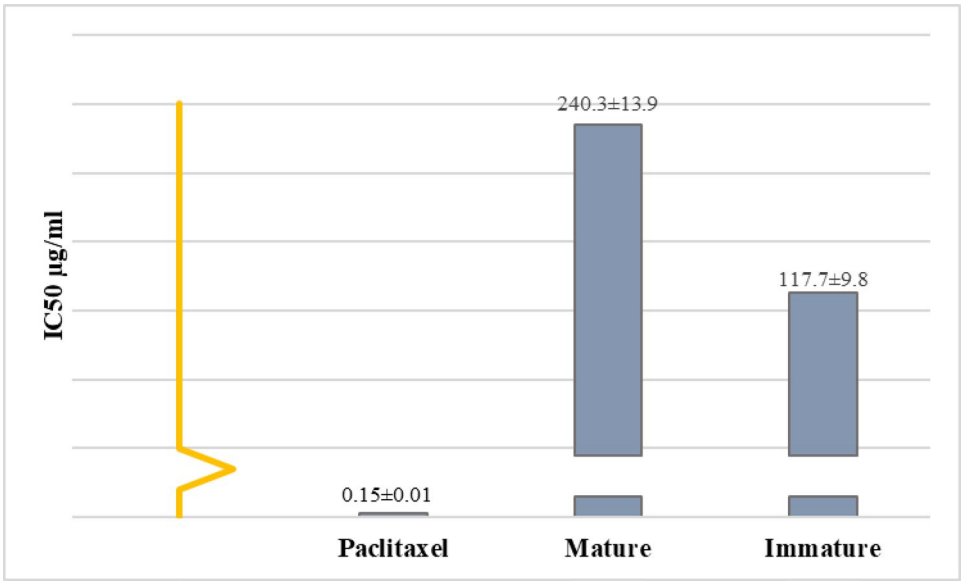

Fig. 7. IC50 values show the effect of *B. aegyptiaca* fruit extracts on cell viability of hepatocellular carcinoma.

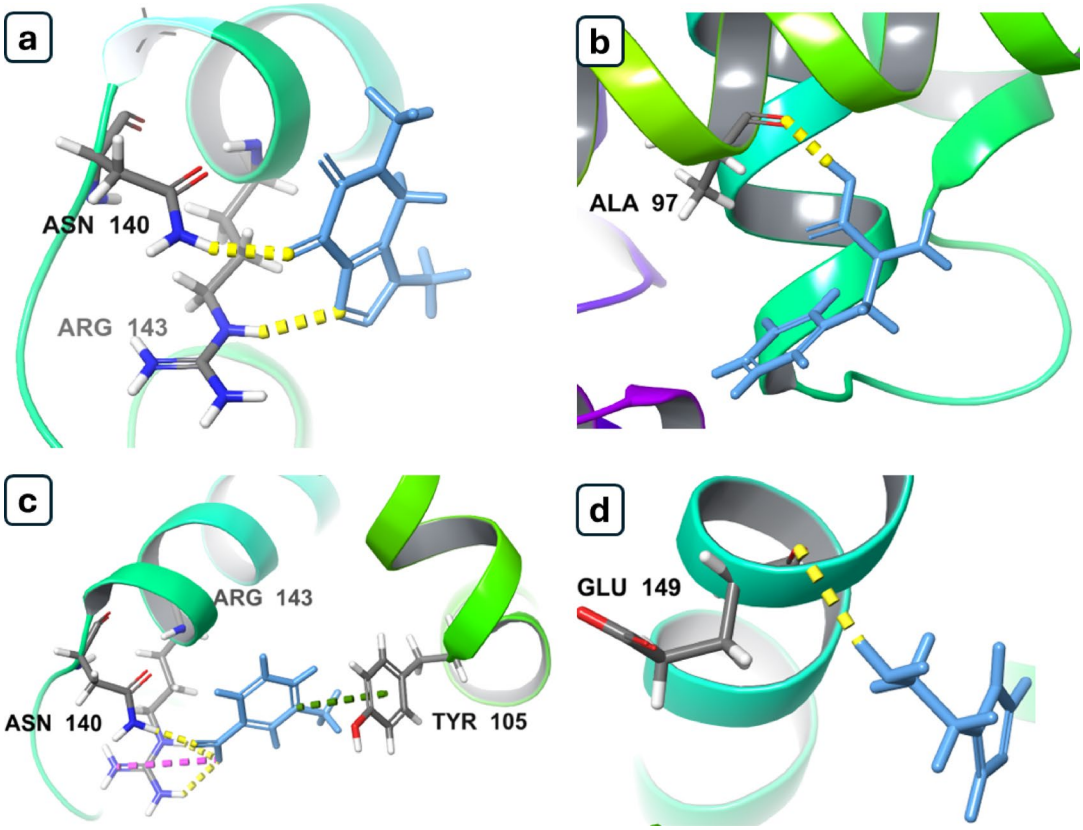

Fig. 8. Binding modes of top compounds from *B. aegyptiaca* fruit extracts against BCL-2 protein: (**a**) theophylline (both immature and mature), (**b**) phenylalanine (immature), (**c**) trigonelline (both immature and mature), (**d**) histamine (immature).

Data availability

The datasets used and/or analyzed during the current study are available from the corresponding author upon reasonable request.

Received: 22 March 2025; Accepted: 6 August 2025
Published online: 23 August 2025

References

1. Chothani, D. L. & Vaghasiya, H. U. A review on *Balanites aegyptiaca* Del (desert date): Phytochemical constituents, traditional uses, and pharmacological activity. *Pharmacogn. Rev.* **5**, 55–62 (2011).
2. Thakkar, V., Dhakad, P. K., Mishra, R. & Gilhotra, R. M. Phytochemical and pharmacological profiling of *Balanites aegyptiaca* Linn.: Exploring the therapeutic potential of a traditional medicinal plant. *Phytomed. Plus* **5**, 100804 (2025).
3. Zein, N., Yassin, F. & Ayoub, H. G. An overview of the phytochemical components, pharmacological action, and therapeutic applications of *Balanites aegyptiaca* Del (desert date). *Biochem. Lett.* **20**, 68–75 (2024).
4. Sagna, M. B. et al. Biochemical composition and nutritional value of *Balanites aegyptiaca* (L.) Del fruit pulps from Northern Ferlo in Senegal. *Afr. J. Biotechnol.* **13**, 336–342 (2014).
5. Perotti, V. E., Moreno, A. S. & Podestá, F. E. Physiological aspects of fruit ripening: The mitochondrial connection. *Mitochondrion* **17**, 1–6 (2014).
6. Forlani, S., Masiero, S. & Mizzotti, C. Fruit ripening: The role of hormones, cell wall modifications, and their relationship with pathogens. *J. Exp. Bot.* **70**, 2993–3006 (2019).
7. Zhu, X., Zhu, Q. & Zhu, H. Towards a better understanding of fruit ripening: Crosstalk of hormones in the regulation of fruit ripening. *Front. Plant Sci.* **14**, 1173877 (2023).
8. Gapper, N. E., McQuinn, R. P. & Giovannoni, J. J. Molecular and genetic regulation of fruit ripening. *Plant Mol. Biol.* **82**, 575–591 (2013).
9. Chaachouay, N., Azeroual, A., Bencharki, B., Douira, A. & Zidane, L. Hormonal interactions during fruit development and ripening. In *Hormonal Cross-Talk, Plant Defense and Development: Plant Biology, Sustainability and Climate Change* (eds Husen, A. & Zhang, W.) 37–46 (Academic Press, 2023).
10. Eladawy, M. L., Basset, H. A., Morsy, M. & Korany, M. H. Study of trend and fluctuations of global solar radiation over Egypt. *NRIAG J. Astron. Geophys.* **10**, 372–386 (2021).
11. Ashour, M. A., El Degwee, Y. A., Hashem, R. H., Abdou, A. A. & Abu-Zaid, T. S. The extent to which the available water resources in upper Egypt can be affected by climate change. *Limnol. Rev.* **24**, 164–177 (2024).
12. Arab, L. et al. Acclimation to heat and drought—Lessons to learn from the date palm (*Phoenix dactylifera*). *Environ. Exp. Bot.* **125**, 20–30 (2016).
13. Van Ploeg, D. & Heuvelink, E. Influence of sub-optimal temperature on tomato growth and yield: A review. *J. Hortic. Sci. Biotechnol.* **80**, 652–659 (2005).

14. Martínez-Rivas, F. J. & Fernie, A. R. Metabolomics to understand metabolic regulation underpinning fruit ripening, development, and quality. *J. Exp. Bot.* **75**, 1726–1740 (2024).
15. Zeng, Q., Chen, J., Zhan, C., Lin, Y. & Chen, Z. Fully exploiting the power of 2D NMR J-resolved spectroscopy. *Anal. Chem.* **92**, 6893–6899 (2020).
16. Ludwig, C. & Viant, M. R. Two-dimensional *J*-resolved NMR spectroscopy: Review of a key methodology in the metabolomics toolbox. *Phytochem. Anal.* **21**, 22–32. https://doi.org/10.1002/pca.1186 (2010).
17. Amberg, A. et al. NMR and MS methods for metabolomics. In *Drug Safety Evaluation. Methods in Molecular Biology* Vol. 1641 (ed. Gautier, J. C.) (Humana Press, 2017). https://doi.org/10.1007/978-1-4939-7172-5_13.
18. Boulos, L. *Flora of Egypt. 3* (Al Hadara Publishing, 2002).
19. Bligh, E. G. & Dyer, W. J. A rapid method of total lipid extraction and purification. *Can. J. Biochem. Physiol.* **37**, 911–917 (1959).
20. Wu, H., Southam, A. D., Hines, A. & Viant, M. R. High-throughput tissue extraction protocol for NMR- and MS-based metabolomics. *Anal. Biochem.* **372**, 204–212 (2008).
21. Pang, Z. et al. MetaboAnalyst 6.0: Towards a unified platform for metabolomics data processing, analysis and interpretation. *Nucleic Acids Res.* **52**, W398–W406 (2024).
22. Farag, M. A. et al. Comparison of *Balanites aegyptiaca* parts: Metabolome providing insights into plant health benefits and valorization purposes as analyzed using multiplex GC–MS, LC–MS, NMR-based metabolomics, and molecular networking. *RSC Adv.* **13**, 21471–21493 (2023).
23. Cook, J. A., VanderJagt, D. J., Pastuszyn, A., Mounkaila, G. & Glew, R. H. Nutrient content of two indigenous plant foods of the western Sahel: *Balanites aegyptiaca* and *Maerua crassifolia*. *J. Food Compos. Anal.* **11**, 221–230 (1998).
24. Kamble, C., Chavan, R. & Kamble, V. A review on amino acids. *Res. Rev. J. Drug Des. Discov.* **8**, 19–27 (2021).
25. Oddy, J., Raffan, S., Wilkinson, M. D., Elmore, J. S. & Halford, N. G. Stress, nutrients and genotype: Understanding and managing asparagine accumulation in wheat grain. *CABI Agric. Biosci.* **1**, 1–14 (2020).
26. Sorrequieta, A., Ferraro, G., Boggio, S. B. & Valle, E. M. Free amino acid production during tomato fruit ripening: A focus on L-glutamate. *Amino Acids* **38**, 1523–1532 (2010).
27. Boggio, S. B., Palatnik, J. F., Heldt, H. W. & Valle, E. M. Changes in amino acid composition and nitrogen metabolizing enzymes in ripening fruits of *Lycopersicon esculentum* Mill. *Plant Sci.* **159**, 125–133 (2000).
28. Pareek, S. Postharvest Ripening Physiology of Crops (ed. Pareek, S.) 12–33 (CRC Press, 2016).
29. Ayvaz Sönmez, D. et al. Phenylalanine ammonialyase and invertase activities in strawberry fruit during ripening progress. *Acta Hortic.* **1309**, 947–954 (2021).
30. Pereira, A. P. A. et al. Impact of ripening on the health-promoting components from fruta-do-lobo (*Solanum lycocarpum* St. Hill). *Food Res. Int.* **139**, 109910 (2021).
31. Regnat, K., Mach, R. L. & Mach-Aigner, A. R. Erythritol as sweetener—Wherefrom and where to?. *Appl. Microbiol. Biotechnol.* **102**, 587–595 (2018).
32. Rapaille, A., Goosens, J. & Heume, M. Sugar alcohols. In *Encyclopedia of Food and Health* (eds Caballero, B. et al.) 211–216 (Academic Press, 2015).
33. Soetan, O. A., Ajao, F. O. & Ajayi, A. F. Blood glucose lowering and anti-oxidant potential of erythritol: An in vitro and in vivo study. *J. Diabetes Metab. Dis.* **22**, 1217–1229 (2023).
34. Li, C. et al. Activation of the calcium signaling, mitogen-activated protein kinase cascade and phenylpropane metabolism contributes to the induction of disease resistance in pear fruit upon phenylalanine treatment. *Postharvest Biol. Technol.* **210**, 112782 (2024).
35. Maoz, I., Lewinsohn, E. & Gonda, I. Amino acids metabolism as a source for aroma volatiles biosynthesis. *Curr. Opin. Plant Biol.* **67**, 102221 (2022).
36. Tieman, D. et al. Tomato aromatic amino acid decarboxylases participate in synthesis of the flavor volatiles 2-phenylethanol and 2-phenylacetaldehyde. *Proc. Natl. Acad. Sci. U.S.A.* **103**, 8287–8292 (2006).
37. Annunziata, M. G., Ciarmiello, L. F., Woodrow, P., Dell'Aversana, E. & Carillo, P. Spatial and temporal profile of glycine betaine accumulation in plants under abiotic stresses. *Front. Plant Sci.* **10**, 230 (2019).
38. Yao, W., Xu, T., Farooq, S. U., Jin, P. & Zheng, Y. Glycine betaine treatment alleviates chilling injury in zucchini fruit (*Cucurbita pepo* L.) by modulating antioxidant enzymes and membrane fatty acid metabolism. *Postharvest Biol. Technol.* **144**, 20–28 (2018).
39. Jia, Z., Wang, Y., Wang, L., Zheng, Y. & Jin, P. Amino acid metabolomic analysis involved in flavor quality and cold tolerance in peach fruit treated with exogenous glycine betaine. *Food Res. Int.* **157**, 111204 (2022).
40. Winter, G., Todd, C. D., Trovato, M., Forlani, G. & Funck, D. Physiological implications of arginine metabolism in plants. *Front. Plant Sci.* **6**, 534 (2015).
41. Gao, H. J., Yang, H. Q. & Wang, J. X. Arginine metabolism in roots and leaves of apple (*Malus domestica* Borkh.): The tissue-specific formation of both nitric oxide and polyamines. *Sci. Hortic.* **119**, 147–152 (2009).
42. Zulfiqar, F. & Ashraf, M. Proline alleviates abiotic stress induced oxidative stress in plants. *J. Plant Growth Regul.* **42**, 4629–4651 (2023).
43. Batista-Silva, W. et al. Modifications in organic acid profiles during fruit development and ripening: Correlation or causation?. *Front. Plant Sci.* **9**, 1689 (2018).
44. Vallarino, J. G. & Osorio, S. Organic acids. In *Postharvest Physiology and Biochemistry of Fruits and Vegetables* (ed. Yahia, E. M.) 207–224 (Woodhead Publishing, 2019).
45. Xi, W., Zheng, H., Zhang, Q. & Li, W. Profiling taste and aroma compound metabolism during apricot fruit development and ripening. *Int. J. Mol. Sci.* **17**, 998 (2016).
46. Zhang, X. et al. Changes in the content of organic acids and expression analysis of citric acid accumulation-related genes during fruit development of yellow (*Passiflora edulis* f. flavicarpa) and purple (*Passiflora edulis* f. edulis) passion fruits. *Int. J. Mol. Sci.* **22**, 5765 (2021).
47. Koshiro, Y., Zheng, X. Q., Wang, M. L., Nagai, C. & Ashihara, H. Changes in content and biosynthetic activity of caffeine and trigonelline during growth and ripening of *Coffea arabica* and *Coffea canephora* fruits. *Plant Sci.* **171**, 242–250 (2006).
48. Wink, M. Plant secondary metabolites modulate insect behavior-steps toward addiction?. *Front. physiol.* **9**, 364 (2018).
49. Pesis, E. The role of the anaerobic metabolites, acetaldehyde and ethanol, in fruit ripening, enhancement of fruit quality and fruit deterioration. *Postharvest Biol. Technol.* **37**, 1–19 (2005).
50. Moyano, E. et al. Comparative study between two strawberry pyruvate decarboxylase genes along fruit development and ripening, post-harvest and stress conditions. *Plant Sci.* **166**, 835–845 (2004).
51. Aslam, M. M. et al. Expression patterns of genes involved in sugar metabolism and accumulation during peach fruit development and ripening. *Sci. Hortic.* **257**, 108633 (2019).
52. Durán-Soria, S., Pott, D. M., Osorio, S. & Vallarino, J. G. Sugar signaling during fruit ripening. *Front. Plant Sci.* **11**, 564917 (2020).
53. Kumar, P. & Dubey, K. K. Citric acid cycle regulation: Back bone for secondary metabolite production. In *New and Future Developments in Microbial Biotechnology and Bioengineering: Microbial Secondary Metabolites Biochemistry and Applications* (eds Gupta, V. K. & Pandey, A.) 165–181 (Elsevier, 2019).
54. Jia, D. et al. Analysis of organic acid metabolism reveals citric acid and malic acid play major roles in determining acid quality during the development of kiwifruit (*Actinidia eriantha*). *J. Sci. Food Agric.* **103**, 6055–6069 (2023).
55. Famiani, F., Battistelli, A., Moscatello, S., Cruz-Castillo, J. G. & Walker, R. P. The organic acids that are accumulated in the flesh of fruits: Occurrence, metabolism and factors affecting their contents—a review. *Rev. Chapingo. Ser. Hortic.* **21**, 97–128 (2015).

56. Tao, H., Sun, H., Wang, Y., Song, X. & Guo, Y. New insights on 'GALA' apple fruit development: sugar and acid accumulation: A transcriptomic approach. *J. Plant Growth Regul.* **39**, 680–702 (2020).
57. Li, X., Li, C., Sun, J. & Jackson, A. Dynamic changes of enzymes involved in sugar and organic acid level modification during blueberry fruit maturation. *Food Chem.* **309**, 125617 (2020).
58. Chang, Y. L., Hsu, Y. J., Chen, Y., Wang, Y. W. & Huang, S. M. Theophylline exhibits anti-cancer activity via suppressing SRSF3 in cervical and breast cancer cell lines. *Oncotarget* **8**, 101461–101474 (2017).
59. Varadarajan, S., Balaji, T. M., Narasimhan, M., Meenakshi, D. P. C. & Sakthisekaran, D. Anticancer activities of *Trigonella foenum-graecum* L. and Trigonelline on an oral squamous cell carcinoma cell line. In *Pharmacological Studies in Natural Oral Care* (eds Chauhan, D. N. et al.) 641–650 (Wiley, 2023).
60. Manivannan, H. P., Veeraraghavan, V. P. & Francis, A. P. Identification of molecular targets of Trigonelline for treating breast cancer through network pharmacology and bioinformatics-based prediction. *Mol. Divers.* **28**, 3835–3857. https://doi.org/10.1007/s11030-023-10780-x (2023).
61. Joondan, N., Laulloo, S. J., Caumul, P. & Kharkar, P. S. Antioxidant, antidiabetic and anticancer activities of L-phenylalanine and L-tyrosine ester surfactants. In vitro and in silico studies of their interactions with macromolecules as plausible mode of action for their biological properties. *Curr. Bioact. Compd.* **15**, 610–622 (2019).
62. Nicoud, M. B. et al. Study of the antitumour effects and the modulation of immune response by histamine in breast cancer. *Br. J. Cancer* **122**, 348–360 (2020).
63. Chen, C. L., Hsu, S. C., Ann, D. K., Yen, Y. & Kung, H. J. Arginine signaling and cancer metabolism. *Cancers* **13**, 3541 (2021).
64. Azab, A. D-Pinitol—Active natural product from carob with notable insulin regulation. *Nutrients* **14**, 1453 (2022).
65. Yao, X. et al. D-Pinitol treatment induced the apoptosis in human leukemia MOLT-4 cells by improved apoptotic signaling pathway. *Saudi J. Biol. Sci.* **27**, 2134–2138 (2020).
66. Srinivasulu, C., Ramgopal, M., Ramanjaneyulu, G., Anuradha, C. M. & Kumar, C. S. Syringic acid (SA)-A review of its occurrence, biosynthesis, pharmacological and industrial importance. *Biomed. Pharmacother.* **108**, 547–557 (2018).
67. Xie, L., Jiang, Y. & Zhou, Q. Theophylline alleviates gentamicin-induced cytotoxicity to sensory hair cells by maintaining HDAC2 expression. *Acta Histochem.* **123**, 151696 (2021).
68. Massari, N. A., Nicoud, M. B. & Medina, V. A. Histamine receptors and cancer pharmacology: An update. *Brit. J. Pharmacol.* **177**, 516–538 (2020).
69. Dev, S., Dhaneshwar, S. R. & Mathew, B. Discovery of camptothecin based topoisomerase I inhibitors: Identification using an atom based 3D-QSAR, pharmacophore modeling, virtual screening and molecular docking approach. *Comb. Chem. High Throughput Scr.* **19**, 752–763 (2016).

Acknowledgements

The authors express gratitude to Dr. Jie Li from the University of South Carolina for his assistance in assigning some compounds.

Author contributions

Study conception and design performed by AA and EM. Material collection and preparations were performed by AA and HA. Metabolites identification and data analysis were performed by AA, AB, and EM. The NMR data collection was performed by AB. In silico study performed by ETM. The first draft of the manuscript was written by AA, HA and EM. All authors revised and approved the final version of the manuscript.

Funding

Open access funding provided by The Science, Technology & Innovation Funding Authority (STDF) in cooperation with The Egyptian Knowledge Bank (EKB). No funding was received for conducting this study. Open access funding is provided by the Science, Technology and Innovation Funding Authority (STDF) in cooperation with The Egyptian Knowledge Bank (EKB).

Declarations

Competing interests

The authors declare no competing interests.

Additional information

Supplementary Information The online version contains supplementary material available at https://doi.org/10.1038/s41598-025-15234-y.

Correspondence and requests for materials should be addressed to A.A.